Dynamic Regulation of Intracellular Labile Cu(I)/Cu(II) Cycle in Microalgae Chlamydomonas reinhardtii

Disrupting the Balance by Cu Stress

Deng, Shaoxi; Wang, Wen-Xiong

Published in:
Environmental Science & Technology

Published: 26/03/2024

Document Version:
Post-print, also known as Accepted Author Manuscript, Peer-reviewed or Author Final version

Published version (DOI):
10.1021/acs.est.3c10257

Publication details:
Deng, S., & Wang, W.-X. (2024). Dynamic Regulation of Intracellular Labile Cu(I)/Cu(II) Cycle in Microalgae *Chlamydomonas reinhardtii*: Disrupting the Balance by Cu Stress. *Environmental Science & Technology*, *58*(12), 5255-5266. https://doi.org/10.1021/acs.est.3c10257

Dynamic regulation of intracellular labile Cu(I)/Cu(II) cycle in microalgae *Chlamydomonas reinhardtii*: Disrupting the balance by Cu stress

Shaoxi Deng[1,2], Wen-Xiong Wang[1,2] *

[1]*School of Energy and Environment and State Key Laboratory of Marine Pollution, City University of Hong Kong, Kowloon, Hong Kong, China*

[2]*Research Centre for the Oceans and Human Health, City University of Hong Kong Shenzhen Research Institute, Shenzhen 518057, China*

*Corresponding author, email: wx.wang@cityu.edu.hk

TOC (prepared by the authors)

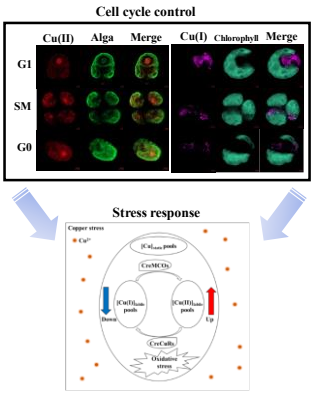

Abstract

The labile metal pool involved in intracellular trafficking and homeostasis is the portion susceptible to environmental stress. Herein, we visualized the different intracellular distributions of labile Cu(I) and Cu(II) pools in the alga *Chlamydomonas reinhardtii.* We first demonstrated that labile Cu(I) predominantly accumulated in the granules within the cytoplasmic matrix, whereas labile Cu(II) pool primarily localized in the pyrenoid and chloroplast. The cell cycle played an integral role in balancing the labile Cu(I)/Cu(II) pools. Specifically, the labile Cu(II) pool primarily accumulated during the SM phase following cell division, while the labile Cu(I) pool dynamically changed during the G phase as cell size increased. Notably, the labile Cu(II) pool in algae at the SM stage exhibited heightened sensitivity to environmental Cu stress. Exogenous Cu stress disrupted the intracellular labile Cu(I)/Cu(II) cycle and balance, causing a shift towards the labile Cu(II) pool. Our proteomic analysis further identified a putative cupric reductase, potentially capable of reducing Cu(II) to Cu(I), and four putative multicopper oxidases, potentially capable of oxidizing Cu(I) to Cu(II), which may be involved in the conversion between labile Cu(I) pool and labile Cu(II) pool. Our study elucidated a dynamic cycle of the intracellular labile Cu(I)/Cu(II) pools, which were accessible and responsive to environmental changes.

Keywords: labile Cu pool, cell cycle, phytoplankton, cupric bioimaging, proteome

One sentence synopsis: Cu stress on microalgae disrupted the dynamic cycle of Cu(I) and Cu(II) with participation of Cu reductases and multicopper oxidases.

1. Introduction

Transition metals such as Cu, Zn and Fe accumulate in the cells owing to their exceptional properties in both architecture and catalysis [1]. These metals orchestrate the processing of biomacromolecules such as DNA, RNA and proteins. They are also integral to some substrate activation through election transfer, often following energy metabolism involving ATP or NADPH. However, an imbalance in intracellular transition metal quota would cause oxidative damage, rendering their redox activity a double-edged sword [2]. Within cells, transition metal sinks are partitioned into two principal pools, including a static pool that is firmly embedded within the active sites of metalloproteins, and a dynamic labile pool weakly coupled with low-molecular-mass (LMM) components [3]. The labile metal pool is responsible for metal ion trafficking from the plasma membrane to their clients, while its destination is considered part of the static pool [4]. As such, the labile metal pool works in metal ion homeostasis and functions in removing free metal and preventing cytotoxic effect, which makes the labile pool susceptible to environmental stress [5, 6].

Copper (Cu) serves as a typical transition metal, but also poses a threat to aquatic ecosystems due to the excessive anthropogenic release of Cu ions [7]. Phytoplankton is sensitive to Cu, and many studies investigated the toxicological effects of Cu stress on algae, but most of these studies primarily focused on the total Cu bioaccumulation [8-10]. Physiologically, intracellular Cu can exist in two oxidation states, Cu(I) and Cu(II), and it displays its redox properties by undergoing reversible transitions between these two states [11]. Like other transition metals, Cu cannot be synthesized by cells. Consequently, labile Cu(I) and Cu(II) pools exist to support the cellular influx, efflux and homeostasis [12].

Chlamydomonas reinhardtii, a unicellular phytoplankton prevalent in various aquatic ecosystems, exhibits sensitive responses to conditions of both metal deficiency and sufficiency, as well as demonstrating a high efficiency for the removal of metal pollutants [13-15]. *Chlamydomonas reinhardtii* predominantly exists as a haploid cell and is equipped with high-quality genome annotations as well as expansive datasets, establishing it as a model organism for environmental toxicological studies [16]. There is increasing interest in the regulation of Cu homeostasis in *Chlamydomonas*. This alga has developed strategies to mitigate Cu deficiency; for example, *Chlamydomonas* preferred replacing Cu-containing plastocyanin with heme-containing cytochrome c_6 to conserve Cu and ensure sufficient availability of Cu for cytochrome oxidase in respiration, suggesting Cu economy under copper deficiency [14]. Wang and Wang recently shed light on the process of intracellular biotransformation of Cu(I)/Cu(II) and its role in cellular toxicity of Cu under Fe deficiency [17].

Moreover, it was suggested that Cu bioaccumulation was simply regulated by the cell cycle [18]. Nevertheless, the mechanisms governing the regulation of labile Cu(I)/Cu(II) pools in *Chlamydomonas*, the fraction of intracellular Cu that is sensitive to external conditions, along with their adaptive responses to environmental stress, remain largely unexplored.

Several methodologies have been developed for the detection of intracellular labile metal pool. For example, a modified liquid chromatography-inductively coupled plasma mass spectrometry (LC-ICP-MS) approach was utilized to study the labile metal pool in *Escherichia coli* [19]. Molecular imaging probes represent an additional innovative strategy, offering high sensitivity and specificity for the visualization of the labile metal pool [20]. In the current study, we firstly visualized the distinct distributions of the labile Cu(I) pool and labile Cu(II) pool in the green algae *Chlamydomonas reinhardtii* with the aid of specific fluorescent probes, and also investigated their rearrangement procedure following cell cycle. Next, we hypothesized the existence of a sophisticatedly regulated labile Cu(I)/Cu(II) cycle within algal cells, and further explored the responses of labile Cu(I)/Cu(II) cycle to environmental stress to test our hypothesis. Subsequently, we conducted a proteomic analysis to elucidate the potential regulatory mechanisms associated with the equilibrium of the labile Cu(I)/Cu(II) cycle. Our study emphasized the significance of the labile Cu pool, rather than merely focusing on robust Cu bioaccumulation, and its modulatory effects on environmental stress. These aspects warrant urgent consideration in future study on environmental toxicity.

Materials and Methods

Experimental materials and algal culture

The green alga *Chlamydomonas reinhardtii* was synchronized using a modified tris-acetate-phosphate (TAP) medium (detailed composition provided in Table S1) at 25 °C under diurnal cycle conditions, consisting of 12 h light and 12 h darkness with a light intensity of 130 μmol photons/m^2/s, in accordance with the method of earlier study [18]. The Cu exposure experiments in this study employed three types of media, designated as Control (Ctr), Low Cu and High Cu, each containing varying concentrations of free Cu ions, with the components listed in Table S1. To prevent contamination, all reusable vessels were soaked in 3% HNO_3 overnight and thoroughly rinsed with ultrapure water to use. A Cu(I) specific fluorescent probe named Cu fluor-4 (CF4), capable of coupling with the intracellular labile Cu(I) pool, and a control probe Cu fluor-4 sulfur 2 (Ctr-CF4-S2), were prepared based on Xiao et al. [21]. The control probe is comparable in size, shape, hydrophobicity, and *in vivo* distribution to the parent Cu(I) probe CF4, but is unresponsive to Cu due to its modified

isosteric receptor. For the detection of intracellular labile Cu(II) pool, we employed a Cu(II)-responsive, activity-based sensing fluorescent probe CD649.2 based on Pezacki et al. [12]. H2DCFDA (2', 7'-dichlorodihydrofluorescein diacetate) (Invitrogen) from Thermo Fisher Scientific was utilized for the detection of reactive oxygen species (ROS) in living algal cells.

Subcellular imaging of algal labile Cu(I)/Cu(II) pool in different cell cycle stages

To investigate the influence of the cell cycle on the regulation of the labile intracellular Cu(I)/Cu(II) cycle, synchronized *Chlamydomonas reinhardtii* cells were collected at various Zeitgeber times (ZT5, ZT14, ZT23 corresponding to G1, SM and G0 phase, respectively) to visualize the subcellular distribution of labile Cu(I)/Cu(II) at different cell cycle stages, as described in our previous work [18]. For Cu(I) staining, algal samples were washed thrice with a rinse medium containing 1 mM Na_2EDTA (detailed composition provided in Table S1) to remove the surface-bound Cu, followed by staining with a 5 μM CF4 probe for 30 min in a PBS solution. Subsequently, the probe was removed, and confocal images were acquired using a Zeiss LSM 900 microscope equipped with Airyscan in channel mode. The excitation wavelength was set at 488 nm, and emissions in the ranges of 530-600 nm and 600-700 nm were recorded to capture Cu(I)-specific and chlorophyll fluorescence-specific emissions, respectively. For Cu(II) staining, the collected algal cells were first rinsed thrice with rinse medium. Since the emission spectrum of the CD649.2 probe (650-700 nm) overlapped with that of chloroplast autofluorescence, the algal pellet was treated with 75% ethanol for 3 min, repeated three times to extract chlorophyll, hence quenching the chloroplast autofluorescence (Figure S1) [22, 23]. The cells were then washed thoroughly with PBS three times to remove the residual ethanol. Afterwards, the algae were incubated with a 5 μM CD649.2 probe and a 5 μM Ctr-CF4-S2 probe together for 1 h. The CD649.2 probe was utilized for staining the intracellular labile Cu(II) pool, while the Ctr-CF4-S2 served to delineate the algal profile. Fluorescence imaging was performed using the Zeiss LSM 900 microscope with Airyscan in channel mode as well. The CD649.2 probe was excited at 633 nm, and emissions between 650-700 nm were collected as Cu(II)-specific signals. For the Ctr-CF4-S2 probe track, excitation was set at 488 nm, with emission collection in the range of 530-600 nm.

Imaging of labile Cu(I)/Cu(II) pools in different cell cycle stages during short-term Cu stress

We gathered alga cells of different cell cycle stages (i.e. G1, SM and G0 phase) separately to conduct three independent exposure experiments. Algae in the G1 phase were subjected to exposure under light conditions, whereas cells in the SM and G0 phase were

exposed under dark conditions. For each exposure experiment, the algal pellets were resuspended in Ctr medium, Low Cu medium or High Cu medium, respectively, to establish different Cu exposure concentrations. The calculated free Cu ion concentrations in Ctr medium, Low Cu medium and High Cu medium were 0, 7.04 and 94.59 nM, respectively (Table S1). The cell density was adjusted to 2×10^6 cells/mL. Following a 2-h exposure period, the cells were harvested and washed three times with rinse medium. Confocal images of labile intracellular Cu(I)/Cu(II) pool were collected following the aforementioned procedure.

Exploring the effects of exogenous Cu stress on labile Cu(I)/(II) cycle.

An additional exposure assay was conducted to investigate the dynamics of the intracellular labile Cu(I)/Cu(II) cycle during exposure, with subsequent relatively quantitative analysis of average unicellular labile Cu(I)/Cu(II) contents using flow cytometry (BD FACS Aria III, Biosciences, USA). In brief, algae in the exponential growth phase were harvested and subsequently exposed to different media (Ctr, Low Cu or High Cu) for 4 h. The cell density was adjusted to 2×10^6 cells / mL. After Cu exposure, the algae were collected and washed three times with rinse medium. A portion of the harvested algae was then prepared for incubation with Cu(I)-specific or Cu(II)-specific probes following the above procedure. For Cu(I) analysis, the Cu(I) signal and chlorophyll fluorescence were detected using the FITC and APC channels, respectively. For Cu(II) analysis, the Cu(II) signal was recorded using the APC channel. Concurrently, a separate aliquot of algae was incubated with the CM-H2DCFDA (10 μM, Invitrogen) fluorescent probe for 30 min to assess ROS level in each group. The fluorescence signal was collected using the FITC channel on the flow cytometry. 10,000 events were analyzed in each flow cytometry assay. The remaining harvested algal samples was used to measure total unicellular Cu bioaccumulation. The cell count of these samples was determined by flow cytometer, after which the algae were digested using 0.5 mL HNO_3 at 80 ^oC for 12 h. The Cu bioaccumulation was ultimately quantified using ICP-MS.

Quantitative proteome analysis

Algal cells in the exponential growth phase were harvested and treated with Ctr or High Cu medium. The cell density was adjusted to 2×10^6 cells / mL. After a 4 h treatment, cells were gathered and washed three times with PBS. Subsequently, the cell pellets were snap-frozen in liquid nitrogen and stored at −80 °C for further sequencing analysis. Total proteins were extracted from the frozen samples using a modified Borax/PVPP/Phenol (BPP) method.

The primary pellets were lysed by the addition of an appropriate volume of protein lysis buffer containing 8 mol / L urea and 1 % sodium dodecyl sulfate, supplemented with a protease inhibitor. The extracted proteins were quantified using the Pierce BCA Protein Assay Kits (Thermo Fisher Scientific). Samples with a total protein content exceeding 100 μg were selected for subsequent analyses. The integrity of the extracted proteins was confirmed by sodium dodecyl sulfate-polyacrylamide gel electrophoresis (SDS-PAGE). An aliquot of 100 μg of high-quality protein samples was dissolved in 100 mM triethylammonium bicarbonate (TEAB) buffer and then digested with trypsin at a 1:50 trypsin-to-protein ratio at 37 ^{o}C. The resulting peptides were labeled with Tandem Mass Tags (TMT, Thermo Fisher Scientific) and subsequently fractionated using high-pH reversed-phase liquid chromatography. The fractionated peptides were ionized and identified via tandem mass spectrometry (MS/MS).

Data analysis

The concentration of free Cu ions in the medium was calculated using Visual MINTEQ 3.1. Confocal images were processed utilizing ZEISS ZEN software version 3.7. Texture analysis of Cu(I)/Cu(II) confocal images was performed using the gray-level co-occurrence matrix (GLCM) method with ImageJ and its plugin Texture Analyzer. Five parameters of texture were calculated: angular second moment (measuring uniformity or homogeneity), GLCM contrast (measuring local variation or local heterogeneity), GLCM correlation (measuring linear dependency), inverse difference moment (measuring local homogeneity) and entropy (measuring randomness or heterogeneity) [24]. Statistical significance was assessed through one-way analysis of variance (ANOVA) followed by Fisher's Least Significant Difference (LSD) test, performed using IBM SPSS Statistics version 25, with a significance threshold set at $p<0.05$ or $p<0.01$. Proteomic data were analyzed using the online platform provided by Majorbio Cloud Platform (www.majorbio.com).

Results and Discussion

Intracellular distribution of labile Cu(I)/Cu(II) pools in green algae.

The intracellular labile Cu(II) pool was firstly imaged in the unicellular green alga *Chlamydomonas reinhardtii* using the Cu(II)-specific probes CD649.2 in our study. Algae cultured in modified TAP medium were gathered during their exponential growth period and subjected to cellular staining. Confocal images revealed that the main fluorescence signals were localized to an alga-specific organelle known as the pyrenoid, with additional signals detected in the extensive, cup-shaped chloroplast region (Figure 1A and B, Figure S2). The

pyrenoid is a non-membrane-bound organelle within the chloroplast that forms through the liquid-liquid phase separation (LLPS) of Ribulose-1,5-bisphosphate carboxylase/oxygenase (Rubisco), as illustrated in Figure S2. Rubisco plays a crucial role in the initial step of CO_2 fixation, and hence pyrenoid contributes to CO_2 concentrating mechanisms (CCMs) that enhance photosynthesis and carbon fixation in green algae [25]. Penen et al. observed an accumulation of Cu signals around pyrenoid region using NanoSIMS in *C. reinhardtii* [26]. Moreover, the green algae *Oocystis nephrocytioides* demonstrated high levels of Cu accumulation around the thylakoids and within the pyrenoid based on Electron Spectroscopic Imaging (ESI) observations [27]. However, these earlier studies did not ascertain the specific form of Cu ions present in the pyrenoid. Herein, for the first time, we document the accumulation of the labile Cu(II) pool within the pyrenoid of *C. reinhardtii*. However, the precise molecular biological role of labile Cu(II) pool within the pyrenoid requires further elucidation.

Subsequently, we investigated the intracellular distribution of the labile Cu(I) pool using the Cu(I)-specific fluorescent probe CF4. In contrast to the labile Cu(II) pool, the labile Cu(I) pool was found to be enriched within several granules around the periphery of the cell or within the cytoplasmic matrix (Figure 1A and B). These areas exhibited a relatively high degree of overlap with the distribution of mitochondria, suggesting a spatial association (Figure S3). Indeed, numerous studies have established a critical link between copper and normal mitochondrial function, particularly with regard to redox regulation and respiration [28]. Castruita et al. found that the mitochondrial cytochrome *c* oxidase COX2A/B was one of the most abundant cuproprotein in transcriptome level in *C. reinhardtii*, which were integral to electron transport [29]. In our prior study, we also confirmed that mitochondria served as the ultimate subcellular repository for hyperaccumulated Cu during the SM phase [18, 30]. In this study, our fluorescence imaging further implied that the labile Cu(I) pool and Cu(II) pools exhibited distinctly different enrichment patterns within green algae. Specifically, the labile Cu(I) pool accumulated within cytoplasmic granules, whereas the labile Cu(II) pool was concentrated within the pyrenoid and chloroplast.

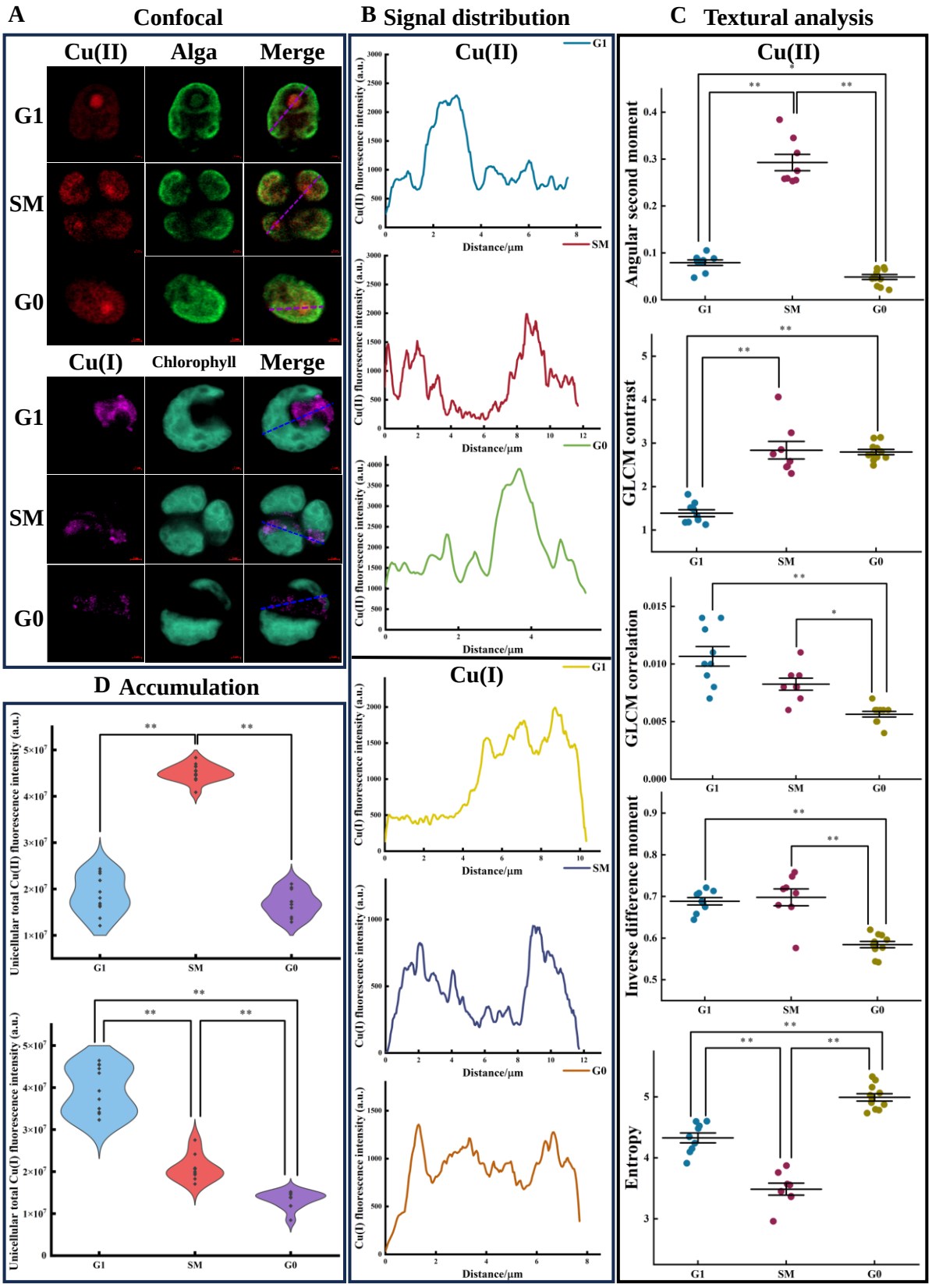

Figure 1. Subcellular distribution of labile Cu(I)/Cu(II) pools. (A) Confocal images show the labile Cu(II) pools and labile Cu(I) pools in different cell cycle stage. (B) Fluorescence signal distribution of labile Cu(II) and Cu(I) along the dashed line in merge channel (A). (C) GLCM

parameters indicate the textural properties of the labile Cu(II) signals during cell cycle. (D) Violin plots describe the unicellular total Cu(II) or Cu(I) fluorescence intensity calculated from confocal images of algal cells in different cell cycle stage (Representatives in A). Dots represent algal cells. ** $p < 0.01$; * $p < 0.05$.

Cell cycle controlled the balance of labile Cu(I)/Cu(II) pools in C. reinhardtii.

Earlier, we showed that cell cycle controlled the uptake and bioaccumulation of Cu in *C. reinhardtii* [18]. Building on this, the present study investigated the dynamic fluctuations of the labile Cu(I)/Cu(II) pools across different cell cycle stages when no Cu stress occurred. Algae were synchronized following our previous study, and algae at different cell cycle stages were collected and stained [18]. The *Chlamydomonas* cell cycle is composed of a prolonged growth phase (G phase), which allows for cell enlargement, and a succession of rapid S phases and mitoses (SM phase), which facilitate the production of daughter cells, therefore we could achieve a high degree of culture synchrony through the modification of light duration and culture medium in a controlled laboratory setting [31-33]. For the labile Cu(II) pool, fluorescence signals were observed to redistribute and evenly partition across daughter cells during the SM phase (Figure 1A and B). The textural analysis revealed an increase in angular second moment and a decrease in entropy during the SM phase, indicative of a more uniform and homogeneous distribution (Figure 1C). These and other textural parameter trends underscore the intricate arrangement of labile Cu(II) throughout the cell cycle. This phenomenon was potentially associated with the concurrent division of chloroplasts and equitable distribution of the pyrenoid during cellular division [34]. After cell division, the small daughter cells exhibited a relatively higher intracellular Cu(II) fluorescence intensity. Intriguingly, it appeared that the labile Cu(II) pool predominantly formed and accumulated during the SM phase, as evidenced by the constancy of total unicellular Cu(II) fluorescence intensity during the G phase and its significant elevation during the SM phase (Figure 1D). Conversely, the labile Cu(I) pool demonstrated relative variability during the G phase in *C. reinhardtii*, with larger cells consistently presenting elevated labile Cu(I) content (Figure 1D) [30]. Additionally, we observed rearrangement and relocation of Cu(I) fluorescence signals during the SM phase, which may be correlated with mitochondrial division (Figure 1A and B) [30, 35]. Subtle alterations in the textural properties of the labile Cu(I) signals during cell cycle were also detected through changes in the GLCM contrast and inverse difference moment, although not in angular second moment and entropy (Figure S4). Therefore, we proposed that the cell cycle governed the equilibrium of the labile Cu(I)/Cu(II) pools. The labile Cu(II) pool remained relatively stable throughout the prolonged G phase and predominantly escalated

during the SM phase in conjunction with cell division, while labile Cu(I) pool dynamically changed during G phase as cell size increase [18].

Labile Cu(II) pool of algae in SM stage showed more sensitive to Cu stress

Many studies posited the cell cycle as a pivotal factor contributing to the phenotypic heterogeneity of cell populations under environmental stressors, including Cu stress. For instance, *Saccharomyces cerevisiae* synchronized at distinct cell cycle stages exhibited heterogeneous resistance to Cu stress [36]. Further, sustained exposure to Cu resulted in cell cycle arrest during the SM phase, underscoring the impact of cell cycle variations [37, 38]. Despite these observations, the mechanisms underlying these effects remain elusive, particularly given the coexistence of both labile Cu(I) and Cu(II) within the cells [12]. To elucidate this, we collected synchronized *C. reinhardtii* at specific cell cycle stages (G0, SM and G1), and exposed them to different Cu concentrations for two hours. After that, fluorescence pictures of labile Cu(I) and Cu(II) pools were gathered for further analysis. It could be shown that the content of labile Cu(II) pool significantly increased across all cell cycle stages under high Cu stress (Figure 2). However, when the Cu concentration was lower in the medium, only cells in the SM phase exhibited an increase in labile Cu(II) content, indicating heightened sensitivity of the labile Cu(II) pool to environmental Cu stress during SM phase. In contrast, the labile Cu(I) pool displayed a markedly different response pattern. The labile Cu(I) content in cells at each cell cycle stage did not exhibit a uniform increasing trend under heightened Cu stress, suggesting functional difference between those two forms (Figure S5). A recent study also found differential cellular toxicity of labile Cu(I) and Cu(II) using Cu-based nanoparticles, suggesting that labile Cu(II) may influence the cell cycle regulation [39]. Thus, we proposed that the heterogeneous resistance of algae at different cell cycle stages to Cu stress stemmed from their disparate sensitivities to the labile Cu(II) pool.

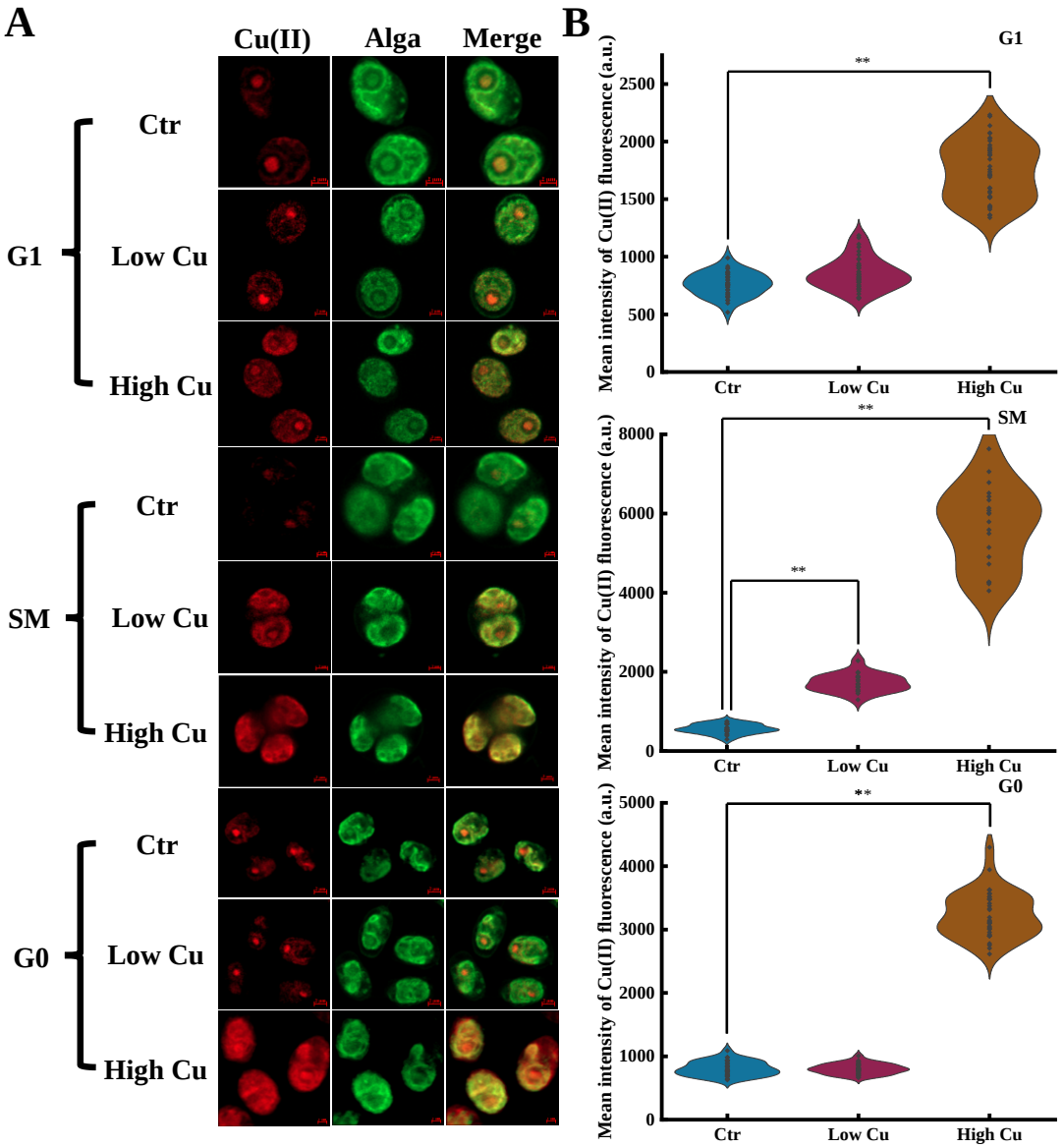

Figure 2. (A) Labile Cu(II) images of algae in different cell cycle stage exposed to different Cu stress. (B) Violin plots describe algal mean intensity of Cu(II) fluorescence collected in images. At least 10 photos were calculated in each group. Dots represent algal cells. ** $p < 0.01$.

Cu stress disrupted intracellular labile Cu(I)/Cu(II) cycle

Our results showed that labile Cu(I) and Cu(II) pools responded differently to Cu stress, as determined using imaging techniques. Given that labile Cu(I) and Cu(II) interconverted within the intracellular Cu(I)/Cu(II) redox cycle, we hypothesized that a cycle existed to maintain the balance of labile Cu(I) and Cu(II) pools, and further explored the influence of environmental Cu stress on this intracellular labile Cu(I)/Cu(II) cycle [12, 17]. Alga cells in the exponential growth period were collected and exposed to different Cu concentrations for 4 h. Flow cytometry was used for the relative quantification of intracellular labile Cu(I)/Cu(II)

contents, while ICP-MS was adopted for the absolute quantification of total Cu bioaccumulation. Eukaryotic cells typically assimilated Cu(I) primarily through the high-affinity Cu permease known as copper transporter 1 (CTR1, also denoted as SLC31A1). Moreover, studies found that the Cu(I) uptake pathway via CTR1 was modulated in response to Cu bioavailability, potentially safeguarding cells against excessive assimilation of Cu(I) through the rapid internalization of CTR1 under environmental Cu stress [18, 40-42]. In contrast, the uptake pathway for Cu(II) was less well-defined. However, some studies proposed divalent metal transporter 1 (DMT1, also known as Nramp2, DCT1 and SLC11A2), a H^+ / divalent metal symporter, as a Cu(II) importer [12, 43-45].

In our study, exposure to elevated environmental Cu stress precipitated a substantial increase in the intracellular labile Cu(II) content, exhibiting an approximately 8-fold increment compared to the ctr group; this was paralleled by a rise in unicellular Cu bioaccumulation, escalating from 14 amol/cell to 185 amol/cell (Figure 2 and 3). The parallel trends between labile Cu(II) pools and Cu bioaccumulation underscore the critical role that labile Cu(II) pools play in the assimilation of Cu by algae. Interestingly, our prior research identified a surge in Cu bioaccumulation during the SM phase of algal cell cycle, which correlatesd with the increment in labile Cu(II) content during the SM phase in the present study (Figure 1D) [18]. However, concomitant with the augmentation of the labile Cu(II) pool was a diminution of the labile Cu(I) pool, likely attributable to an aberrant enhancement of the intracellular oxidative milieu. This was further evidenced by a roughly two-fold increase in ROS content within the high Cu group relative to the ctr group, which corroborated the escalated intracellular oxidative stress. Our data showed that the labile Cu(I) pool decreased by 80% in the high Cu stress group compared with the ctr group. Normally, the intracellular labile Cu(I)/Cu(II) cycle was equilibrated by chelators such as glutathione (GSH), the metallothioneins (MTs) system, and ascorbate, which collectively fostered a conducive redox environment through Fenton-like reactions [46-48]. Given that Cu(I) exhibited a pro-oxidant property by supporting one-electron redox transitions, potentially engendering harmful radical species, Cu(II) was considered the less toxic form of Cu [49]. Consequently, in response to environmental Cu stress, cells appeared to modulate the labile Cu(I)/Cu(II) cycle in favor of the labile Cu(II) pool as a detoxification measure. Our study strongly suggested that exogenous Cu stress would break the intracellular labile Cu(I)/Cu(II) cycle, leading to an anomalous surge in labile Cu(II) content and a corresponding reduction in labile Cu(I) levels.

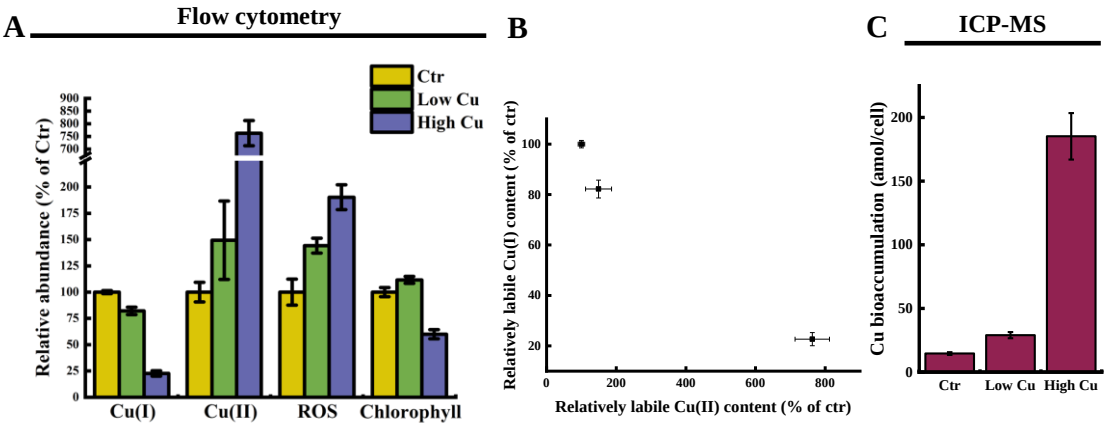

Figure 3. (A) Diverse fluorescent parameters measured via flow cytometry. Fluorescence intensity is normalized by dividing the average fluorescence intensity in ctr group. (B) Scatter diagram illustrates the relationship between labile Cu(I) pool and labile Cu(II) pool. (C) Unicellular total Cu bioaccumulation determined by ICP-MS. Algal cell number in samples are calculated using flow cytometry.

Cu stress caused functional disorders in mitochondria and chloroplast

Proteomic background of algae in Cu stress were analyzed to explore the possible regulation pathway involving in labile Cu(I)/Cu(II) cycle. Functional annotation of the raw data was based on the reference proteome library of *Chlamydomonas reinhardtii* (UP000006906) found in the UniProt database. Overall, a total of 1387 differentially expressed proteins (DEPs), comprising 827 up-regulated proteins (URPs) and 560 down-regulated proteins (DRPs), which emerged as significantly enriched in our dataset (Figure S7). Subcellular localization predictions for DEPs indicated a predominance in mitochondria and chloroplasts, which respectively contained 18.84 % and 18.10 % of the DEPs when compared with other organelles (Figure 4A). Meanwhile, Gene Ontology (GO) terms "mitochondrial protein – containing complex" and KEGG pathway "photosynthesis" were also found to be significantly enriched, highlighting a strong correlation to the functional activities of mitochondria and chloroplasts (Figure 4B and C). Additionally, mitochondria and chlorophyll content were also influenced by Cu stress (Figure 3A) [30]. Thus, our study indicated that Cu stress caused functional disorders in both mitochondria and chloroplast.

Next, we screened for candidates of putative metallothioneins within the protein annotation library and the set of DEPs using the keyword "metal ion binding". In total, 843 proteins were identified as putative metallothionein candidates, with 212 exhibiting differential expression. Notably, these differentially expressed putative metallothioneins displayed distinct expression pattern: subcluster 1, comprising 99 proteins, was down-regulated, whereas subcluster 2, consisting of 113 proteins, was up-regulated in the Cu group

(Figure 4D and E). Subsequently, we conducted a gene set enrichment analysis (GSEA) on the putative metallothionein protein set, using the protein annotation library from this study as a priori defined protein set S [50]. The GSEA revealed that the GO term "GO:0051536 iron-sulfur cluster binding" —which pertains to the binding of iron-sulfur clusters, an amalgam of iron and sulfur atoms—was significantly down-regulated in the Cu group (p-value = 0.021, normalized enrichment score (NES) = -1.141). Correspondingly, the GO term "GO:0005507 Cu ion binding" was significantly up-regulated in the Cu group (p-value = 0.034, NES = 1.544), suggesting diverse responses of metal species binding proteins to the imbalance of the labile Cu(I)/Cu(II) cycle (Figure 5A and B). Intriguingly, a Venn diagram comparison of the differentially expressed putative metallothionein subclusters and the core enrichment protein set (also referred to as the leading-edge subset) from the GSEA of GO:0005507 revealed that more than half of the core enrichment proteins associated with copper ion binding were not differentially expressed in the Cu group. However, the GSEA indicated that these proteins played a significant role in the up-regulation of the GO term "GO:0005507" (Figure 5C). Previous study also confirmed the abnormal regulation of labile Cu(I)/Cu(II) cycle under Fe deficiency and Zn deficiency, thus we inferred that the regulation of labile Cu(I)/Cu(II) pool was tightly correlated to the labile pool of other transient metal ions, such as iron [17].

A novel cytoplasmic cupric reductase and multicopper oxidases annotated involved in regulation of labile Cu(I)/Cu(II) cycle

Notably, a putative cupric reductase (UniProt accession number: *A8IUR7*, named CreCuR1 in this study) was identified as it was categorized under the GO term "GO: 0008823 cupric reductase activity", and subcellular localization prediction analysis revealed that it was a cytoplasmic protein. Further sequence domain analysis conducted on the Pfam platform showed that CreCuR1 aligned with the DUDULIN-RELATED (PTHR14239) family in the PANTHER knowledgebase (Figure 4F and S9). Orthologs of this family in mammals, such as Steap2-4, and the analogous yeast FRE proteins, have functional roles as cupric reductases [51-53]. Typically, cupric reductases are localized to the plasma membrane where they facilitate the reduction of Cu(II) to Cu(I), subsequently delivering Cu(I) to the copper transporter CTR in conjunction with the dehydrogenation of NAD(P)H. However, recent studies also provided evidence for the existence of cytoplasmic cupric reductases and their role in maintaining the intracellular labile Cu(I) pool [54, 55]. Although CreCuR1 did not exhibit a significant fold change (FC = 0.883) to be classified as a DEP, protein-protein interaction network analysis (PPI-Net) revealed direct interactions with COX2A/B (*Q9AYR9*

and *Q9AU05*) and FOX1 (*Q8LL91*), and indirect interactions with other core copper-binding proteins, including the Cu(I) importers CTR1/2 (Figure 5D). COX2 is an integral membrane subunit of cytochrome *c* oxidase that plays a role in respiration within the inner mitochondrial membrane, where labile Cu(I) signals accumulate. FOX1 was known as a multicopper ferroxidase necessary for iron assimilation and was one of the most transcriptionally abundant cuproproteins in *Chlamydomonas* [56]. Thus, our results suggested that this novel cytoplasmic cupric reductase, CreCuR1, may be involved in sustaining the intracellular labile Cu(I) pool.

FOX1 is a multicopper oxidase (MCO) that has been extensively studied in *Chlamydomonas* and is associated with the Cu chaperone ATX1 and a Cu(I)-transporting P-type ATPase (*A0A2K3CU24*, referred to as CTP1 in this study) through the secretory pathway for Cu handling [57]. MCOs are a diverse group of enzymes that typically incorporate four Cu atoms—one type I Cu, one type II Cu, and a pair of type III Cu centers—and utilize Cu ions as cofactors to catalyze the oxidation of substrates such as phenols, bilirubin, and ascorbate [58]. Furthermore, the Cu efflux oxidase (CueO) subcluster of the MCO family was believed to confer Cu tolerance in bacteria by oxidizing the more toxic Cu(I) to the less reactive Cu(II), thereby protecting periplasmic proteins [59]. Yeast multicopper ferroxidase Fet3 and human ceruloplasmin, also members of the MCO family, were confirmed to possess robust catalysts of the oxidation of Cu(I) to Cu(II), and involved in maintaining the steady-state level of Cu(I) content [60, 61]. In our study, PPI-Net analysis revealed that FOX1 directly interacted with CTP2 and CTP4 (*A0A2K3D9E7* and *A0A2K3D994*, respectively), which were involved in delivering Cu to plastocyanin for photosynthesis in the thylakoid lumen. It also interacted with the mitochondrial Cu-binding metallochaperone SCO1 and COX2A/B, which were implicated in respiration and the electron transport chain in the mitochondrial inner membrane, as well as with the Cu(I) importer CTR1, suggesting a role for FOX1 in the labile Cu(I)/Cu(II) cycle (Figure 5D) [62]. Beyond FOX1, three additional proteins were annotated as putative MCOs in our study, identified by their structural Cu oxidase domains present in the Pfam platform—CreMCO1 (*A0A2K3E6T3*), CreMCO2 (*A0A2K3D4U3*), and CreMCO3 (*A0A2K3DGH0*; Figure 4F). CreMCO1 and CreMCO2 were notably up-regulated in the Cu-treated group. The PPI-Net analysis indicated that both CreMCO1 and CreMCO2 directly interacted with CTP1/2/4 and SCO1. However, CreMCO3 did not show significant enrichment, suggesting functional divergence among the MCOs (Figure 5D). Significantly, CreMCO2 was also found to directly interact with CTR2, another membrane-localized Cu(I) importer in *Chlamydomonas* [41], highlighting a potentially intricate network of Cu trafficking

and labile Cu(I)/Cu(II) cycle mediated by these MCOs.

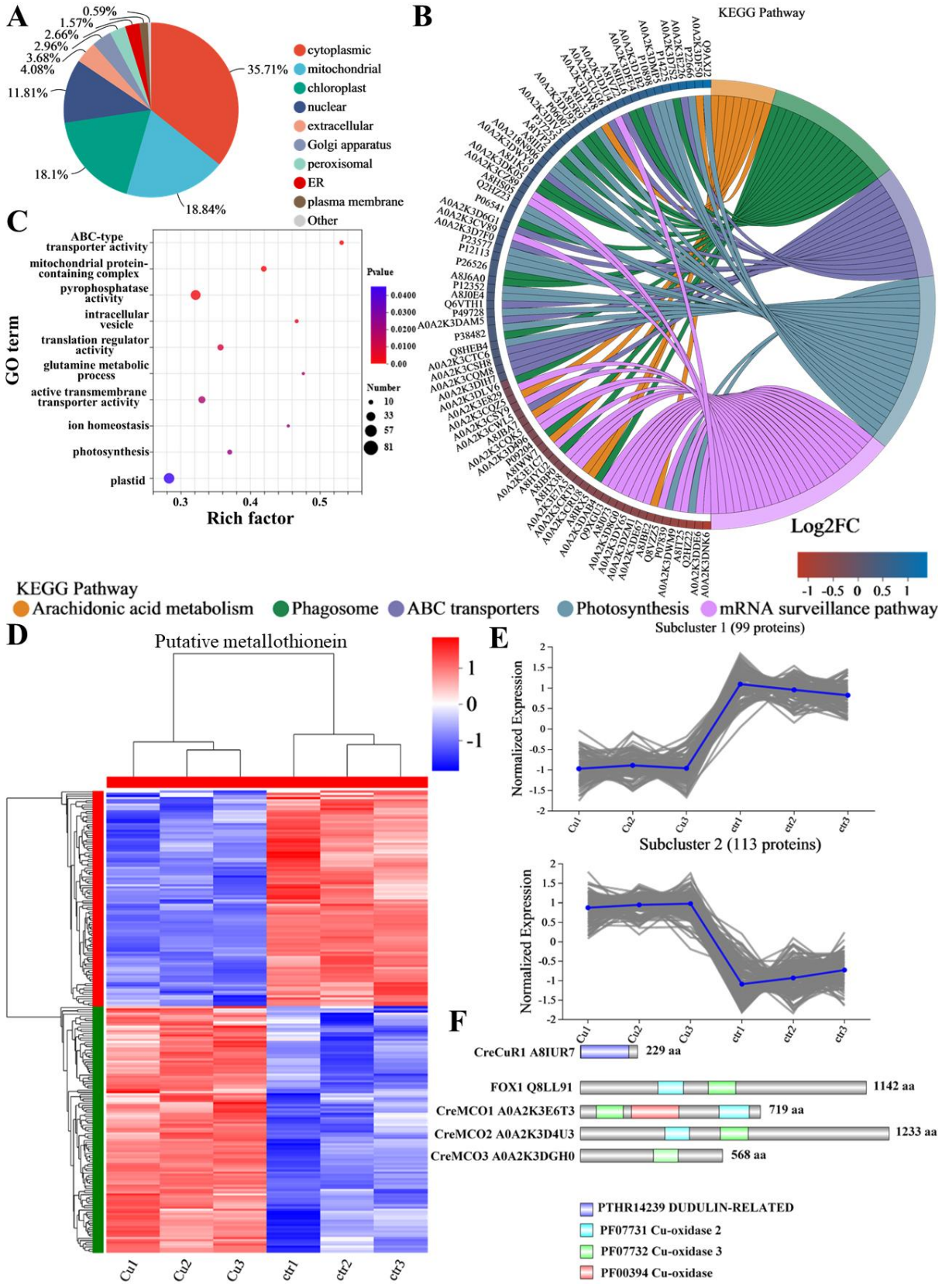

Figure 4. (A) Pie chart describes the subcellular localization annotation of DEPs. (B) Chord diagram visualizes the top 5 KEGG pathways enriched in KEGG enrichment analysis. DEPs in those KEGG pathways are listed in the left sorting by log_2FC value. (C) Bubble diagram

exhibits part of GO terms significantly enriched in Gene Ontology Enrichment analysis. Clustering heatmap (D) shows the expression pattern of 212 deduced metallothionein, and line charts (E) show the expression tendency of putative metallothionein in two subclusters. Each gray line represents one member protein, and the blue line indicates the average expression level of proteins in the subcluster. (F) Diagram demonstrates the protein domain of CreCuR1, FOX1, CreMCO1/2/3.

ABC transporters worked in the balance of labile Cu(I)/Cu(II) cycle

Our study found significant enrichment of ATP-binding cassette (ABC) transporters among DEPs, as indicated by GO terms and KEGG pathway enrichment analyses (GO:0140359 "ABC-type transporter activity" and cre02010 "ABC transporters", respectively; Figure 4B and C). This suggested a role for ABC transporters in the balance of the labile Cu(I)/Cu(II) cycle. ABC transporters constitute a broad family of proteins that facilitate the transport of a variety of substrates, powered by ATP hydrolysis. Many studies emphasized the relationship between ABC transporters and Cu stress across different species [63-65]. Thus, we conducted a GSEA specifically on the KEGG pathway item cre02010 "ABC transporters". This pathway was found to be significantly activated in the Cu-exposed group (p-value = 0.005, NES = 1.754), with sixteen putative ABC transporters identified as leading-edge proteins, underscoring their potential importance (Figures 5A and B). One of these, CDS1 (*Q6VTH1*), was identified as a mitochondrial ABC transporter known to be involved in cadmium tolerance [66]. Although the functional annotation of the remaining fifteen putative ABC transporters is not well understood, our subcellular localization analysis predicted their distribution across various organelles—including mitochondria, chloroplasts, the Golgi apparatus, and the endoplasmic reticulum (Table S4). This suggested a potential role for these transporters in trafficking the intracellular labile Cu pools.

Oxidative stress often triggers cellular functional disorders at various levels. The imbalance of intracellular labile Cu(I)/Cu(II) cycle was also followed by oxidative stress described above (Figure 3A). Besides, KEGG pathway item mRNA surveillance pathway (CRE03015) was also significantly enriched in our study (Figure 4B). This pathway represents a quality control mechanism that detects and degrades aberrant mRNAs, thereby preventing the translation of potentially harmful proteins. Previous research showed that disruption of the mRNA surveillance pathway could lead to increased protein aggregation in yeast [67]. In our study, GSEA revealed that the mRNA surveillance pathway was also suppressed in the Cu-exposed group (p-value = 0, NES = -2.324; Figure 5A). This suppression could potentially result in increased abnormal protein formation and protein aggregation. Furthermore, KEGG pathway (like cre00590 arachidonic acid metabolism) and

GO term (like GO:0006541 glutamine metabolic process) involved in the immune system function, were also significantly enriched, supporting the occurrence of immune response under Cu stress (Figure 4B and C).

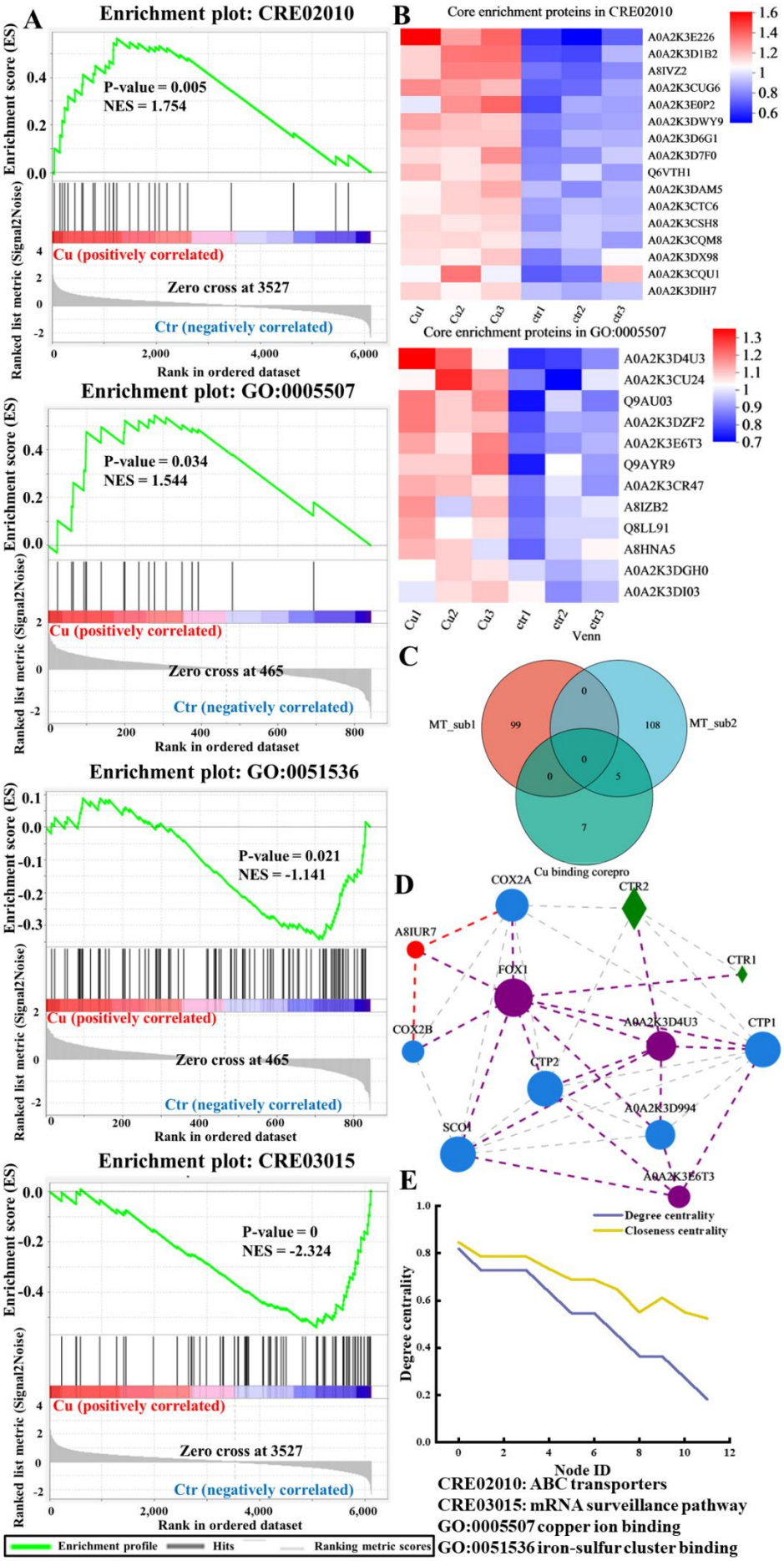
A
Enrichment plot: CRE02010
P-value = 0.005
NES = 1.754
Cu (positively correlated)
Zero cross at 3527
Ctr (negatively correlated)
Enrichment score (ES)
Ranked list metric (Signal2Noise)
Rank in ordered dataset
Enrichment plot: GO:0005507
P-value = 0.034
NES = 1.544
Cu (positively correlated)
Zero cross at 465
Ctr (negatively correlated)
Enrichment score (ES)
Ranked list metric (Signal2Noise)
Rank in ordered dataset
Enrichment plot: GO:0051536
P-value = 0.021
NES = -1.141
Cu (positively correlated)
Zero cross at 465
Ctr (negatively correlated)
Enrichment score (ES)
Ranked list metric (Signal2Noise)
Rank in ordered dataset
Enrichment plot: CRE03015
P-value = 0
NES = -2.324
Cu (positively correlated)
Zero cross at 3527
Ctr (negatively correlated)
Enrichment score (ES)
Ranked list metric (Signal2Noise)
Rank in ordered dataset
Enrichment profile
Hits
Ranking metric scores
B
Core enrichment proteins in CRE02010
A0A2K3E226
A0A2K3D1B2
A8IVZ2
A0A2K3CUG6
A0A2K3E0P2
A0A2K3DWY9
A0A2K3D6G1
A0A2K3D7F0
Q6VTH1
A0A2K3DAM5
A0A2K3CTC6
A0A2K3CSH8
A0A2K3CQM8
A0A2K3DX98
A0A2K3CQU1
A0A2K3DIH7
Cu1
Cu2
Cu3
ctr1
ctr2
ctr3
Core enrichment proteins in GO:0005507
A0A2K3D4U3
A0A2K3CU24
Q9AU03
A0A2K3DZF2
A0A2K3E6T3
Q9AYR9
A0A2K3CR47
A8IZB2
Q8LL91
A8HNA5
A0A2K3DGH0
A0A2K3DI03
Venn
C
MT_sub1
MT_sub2
Cu binding corepro
D
COX2A
CTR2
A8IUR7
CTR1
FOX1
COX2B
A0A2K3D4U3
CTP1
CTP2
A0A2K3D994
SCO1
A0A2K3E6T3
E
Degree centrality
Closeness centrality
Node ID
CRE02010: ABC transporters
CRE03015: mRNA surveillance pathway
GO:0005507 copper ion binding
GO:0051536 iron-sulfur cluster binding

Figure 5. (A) GSEA results of GO terms and KEGG pathways. (B) Heatmaps show the expression pattern of leading-edge subsets enriched in GSEA. (C) Venn diagram compares the putative metallothionein subclusters and leading-edge subset enriched in the GSEA of GO:0005507. (D) Protein interaction network diagram shows the interaction between cupric reductase, multiCu oxidases and other core proteins in Cu influx and efflux system. (E) Distribution map of nodes centrality in PPI-Net (D). Node represents protein. Degree centrality describes the number of edges incident upon a node. Closeness centrality describes the average path length of one node to other nodes in PPI-Net.

Our study demonstrated for the first time that labile Cu(I) and Cu(II) pools exhibited different intracellular distributions in algal cells, and that the cell cycle regulated the rearrangement of labile Cu(I)/Cu(II) pools throughout growth and proliferation. We observed that the labile Cu(II) pool in the SM stage was more sensitive to environmental Cu stress. Furthermore, exposure to Cu stress disrupted the balance of the intracellular Cu(I)/Cu(II) cycle, shifting the dynamics towards an increased labile Cu(II) pool alongside a concomitant decrease in the labile Cu(I) pool. Mechanistically, our proteomic analysis suggested that a novel cytoplasmic cupric reductase and multicopper oxidases may contribute to the intracellular transformation between labile Cu(I) and Cu(II). Cu as a representative transition metal orchestrates the normal cellular function, but becomes toxic if overloaded. Previous studies primarily focused on determining the intracellular Cu quota as a measure of bioaccumulation to assess toxicity, often overlooking the heterogeneous response of different Cu species. Our study concentrated on the labile Cu(I)/Cu(II) pools—those fractions of the Cu quota that are accessible to the external environment—and confirmed their traceable response to Cu stress. Our results provided a novel perspective for future studies in environmental toxicology, emphasizing the importance of considering labile metal pools in the assessment of metal toxicity.

Acknowledgement

We thank Prof. Christopher Chang, University of California at Berkeley, USA, for the donations of Cu probes in this study. This study was supported by a GRF grant from Hong Kong Research Grants Council (CityU 11102321).

Supporting information

Enlarged optical micrograph and diagram illustrates the subcellular structure of green algae *Chlamydomonas reinhardtii.* Subcellular distribution of mitochondria in algal cells. Textural analysis of the labile Cu(I) signals during cell cycle. Labile Cu(I) images of algae in different cell cycle stage collected under Cu stress. Identification and analysis of the raw data of proteome. PCA analysis representing the variation of translational background in samples.

Volcano map showing the DEPs identified in proteome data. Upset diagram showing the functional annotation of identified proteins to different databases. Heatmap illustrating the expression pattern of all DEPs identified in this study. Functionally conserved domains and motifs of CreCUR1 and HsaSteap2-4. Table lists the composition of different medium. Tables about the node information and nodes centrality in protein-protein interaction network. Subcellular localization analysis of 16 core candidates of ABC transporter enriched in GSEA.

References

1. Finney, L. A.; O'Halloran, T. V., Transition metal speciation in the cell: insights from the chemistry of metal ion receptors. *Science* **2003,** *300*, (5621), 931-6.
2. Imlay, J. A., Pathways of oxidative damage. *Annu Rev Microbiol* **2003,** *57*, 395-418.
3. Ackerman, C. M.; Lee, S.; Chang, C. J., Analytical methods for imaging metals in biology: from transition metal metabolism to transition metal signaling. *Anal Chem* **2017,** *89*, (1), 22-41.
4. Banci, L.; Bertini, I.; Ciofi-Baffoni, S.; Kozyreva, T.; Zovo, K.; Palumaa, P., Affinity gradients drive copper to cellular destinations. *Nature* **2010,** *465*, (7298), 645-8.
5. Valko, M.; Rhodes, C. J.; Moncol, J.; Izakovic, M.; Mazur, M., Free radicals, metals and antioxidants in oxidative stress-induced cancer. *Chem Biol Interact* **2006,** *160*, (1), 1-40.
6. Cotruvo, J. A., Jr.; Aron, A. T.; Ramos-Torres, K. M.; Chang, C. J., Synthetic fluorescent probes for studying copper in biological systems. *Chem Soc Rev* **2015,** *44*, (13), 4400-14.
7. Pan, K.; Wang, W.-X., Trace metal contamination in estuarine and coastal environments in China. *Sci Total Environ* **2012,** *421-422*, 3-16.
8. Kalinowska, R.; Pawlik-Skowronska, B., Response of two terrestrial green microalgae (Chlorophyta, Trebouxiophyceae) isolated from Cu-rich and unpolluted soils to copper stress. *Environ Pollut* **2010,** *158*, (8), 2778-85.
9. Jamers, A.; Blust, R.; De Coen, W.; Griffin, J. L.; Jones, O. A., Copper toxicity in the microalga *Chlamydomonas reinhardtii*: an integrated approach. *Biometals* **2013,** *26*, (5), 731-40.
10. Liu, S.; Li, J.; Oshita, S.; Kamruzzaman, M.; Cui, M.; Fan, W., Formation of a hydrogen radical in hydrogen nanobubble water and its effect on copper toxicity in Chlorella. *ACS Sustain Chem Eng* **2021,** *9*, (33), 11100-11109.
11. Solomon, E. I.; Sundaram, U. M.; Machonkin, T. E., Multicopper oxidases and oxygenases. *Chem Rev* **1996,** *96*, (7), 2563-2606.
12. Pezacki, A. T.; Matier, C. D.; Gu, X.; Kummelstedt, E.; Bond, S. E.; Torrente, L.; Jordan-Sciutto, K. L.; DeNicola, G. M.; Su, T. A.; Brady, D. C.; Chang, C. J., Oxidation state-specific fluorescent copper sensors reveal oncogene-driven redox changes that regulate labile copper(II) pools. *Proc Natl Acad Sci U S A* **2022,** *119*, (43), e2202736119.
13. Blaby-Haas, C. E.; Merchant, S. S., The ins and outs of algal metal transport. *Biochim Biophys Acta* **2012,** *1823*, (9), 1531-52.
14. Merchant, S. S.; Schmollinger, S.; Strenkert, D.; Moseley, J. L.; Blaby-Haas, C. E., From economy to luxury: Copper homeostasis in Chlamydomonas and other algae. *Biochim Biophys Acta Mol Cell Res* **2020,** *1867*, (11), 118822.
15. Flouty, R.; Estephane, G., Bioaccumulation and biosorption of copper and lead by a

580 unicellular algae *Chlamydomonas reinhardtii* in single and binary metal systems: a
581 comparative study. *J Environ Manage* **2012,** *111*, 106-14.
582 16. Dupuis, S.; Merchant, S. S., *Chlamydomonas reinhardtii*: a model for photosynthesis and
583 so much more. *Nat Methods* **2023,** *20*, (10), 1441-1442.
584 17. Wang, X.; Wang, W.-X., Intracellular biotransformation of Cu(II)/Cu(I) explained high Cu
585 toxicity to phytoplankton *Chlamydomonas reinhardtii*. *Environ Sci Technol* **2021,** *55*, (21),
586 14772-14781.
587 18. Deng, S.; Wang, W.-X., A surge of copper accumulation in cell division revealed its
588 cyclical kinetics in synchronized green alga *Chlamydomonas reinhardtii*. *Sci Total Environ*
589 **2023,** *899*, 165566.
590 19. Brawley, H. N.; Lindahl, P. A., Direct detection of the labile nickel pool in *Escherichia*
591 *coli*: new perspectives on labile metal pools. *J Am Chem Soc* **2021,** *143*, (44), 18571-18580.
592 20. Pham, V. N.; Chang, C. J., Metalloallostery and transition metal signaling: bioinorganic
593 copper chemistry beyond active sites. *Angew Chem Int Ed Engl* **2023,** *62*, (11), e202213644.
594 21. Xiao, T.; Ackerman, C. M.; Carroll, E. C.; Jia, S.; Hoagland, A.; Chan, J.; Thai, B.; Liu, C.
595 S.; Isacoff, E. Y.; Chang, C. J., Copper regulates rest-activity cycles through the locus
596 coeruleus-norepinephrine system. *Nat Chem Biol* **2018,** *14*, (7), 655-663.
597 22. Ritchie, R. J., Consistent sets of spectrophotometric chlorophyll equations for acetone,
598 methanol and ethanol solvents. *Photosynth Res* **2006,** *89*, (1), 27-41.
599 23. Zhou, X.; Carranco, R.; Vitha, S.; Hall, T. C., The dark side of green fluorescent protein.
600 *New Phytol* **2005,** *168*, (2), 313-22.
601 24. Haralick, R. M.; Shanmugam, K.; Dinstein, I. H., Textural features for image classification.
602 *IEEE Transactions on Systems, Man, and Cybernetics* **1973,** *SMC-3*, (6), 610-621.
603 25. Barrett, J.; Girr, P.; Mackinder, L. C. M., Pyrenoids: CO_2-fixing phase separated liquid
604 organelles. *Biochim Biophys Acta Mol Cell Res* **2021,** *1868*, (5), 118949.
605 26. Penen, F.; Malherbe, J.; Isaure, M. P.; Dobritzsch, D.; Bertalan, I.; Gontier, E.; Le
606 Coustumer, P.; Schaumloffel, D., Chemical bioimaging for the subcellular localization of trace
607 elements by high contrast TEM, TEM/X-EDS, and NanoSIMS. *J Trace Elem Med Biol* **2016,**
608 *37*, 62-68.
609 27. Soldo, D.; Hari, R.; Sigg, L.; Behra, R., Tolerance of *Oocystis nephrocytioides* to copper:
610 intracellular distribution and extracellular complexation of copper. *Aquat Toxicol* **2005,** *71*, (4),
611 307-17.
612 28. Ruiz, L. M.; Libedinsky, A.; Elorza, A. A., Role of copper on mitochondrial function and
613 metabolism. *Front Mol Biosci* **2021,** *8*, 711227.
614 29. Castruita, M.; Casero, D.; Karpowicz, S. J.; Kropat, J.; Vieler, A.; Hsieh, S. I.; Yan, W.;
615 Cokus, S.; Loo, J. A.; Benning, C.; Pellegrini, M.; Merchant, S. S., Systems biology approach
616 in Chlamydomonas reveals connections between copper nutrition and multiple metabolic steps.
617 *Plant Cell* **2011,** *23*, (4), 1273-92.
618 30. Wang, X.; Wang, W.-X., Cell cycle-dependent Cu uptake explained the heterogenous
619 responses of Chlamydomonas to Cu exposure. *Environ Pollut* **2023,** *319*, 121013.
620 31. Cross, F. R.; Umen, J. G., The Chlamydomonas cell cycle. *Plant J* **2015,** *82*, (3), 370-392.
621 32. Zones, J. M.; Blaby, I. K.; Merchant, S. S.; Umen, J. G., High-resolution profiling of a

synchronized diurnal transcriptome from *Chlamydomonas reinhardtii* reveals continuous cell and metabolic differentiation. *Plant Cell* **2015,** *27*, (10), 2743-69.
33. Heldt, F. S.; Tyson, J. J.; Cross, F. R.; Novak, B., A single light-responsive sizer can control multiple-fission cycles in Chlamydomonas. *Curr Biol* **2020,** *30*, (4), 634-644 e7.
34. Oleksienko, A. A.; Kot, Y. G.; Komaristaya, V. P., DNA-specific DAPI staining of the pyrenoid matrix during its fission in *Dunaliella salina* (Dunal) Teodoresco (Chlorophyta). *Curr Microbiol* **2020,** *77*, (11), 3450-3459.
35. Imoto, Y.; Fujiwara, T.; Yoshida, Y.; Kuroiwa, H.; Maruyama, S.; Kuroiwa, T., Division of cell nuclei, mitochondria, plastids, and microbodies mediated by mitotic spindle poles in the primitive red alga *Cyanidioschyzon merolae*. *Protoplasma* **2010,** *241*, (1-4), 63-74.
36. Sumner, E. R.; Avery, A. M.; Houghton, J. E.; Robins, R. A.; Avery, S. V., Cell cycle- and age-dependent activation of Sod1p drives the formation of stress resistant cell subpopulations within clonal yeast cultures. *Mol Microbiol* **2003,** *50*, (3), 857-70.
37. Thit, A.; Selck, H.; Bjerregaard, H. F., Toxicity of CuO nanoparticles and Cu ions to tight epithelial cells from *Xenopus laevis* (A6): effects on proliferation, cell cycle progression and cell death. *Toxicol In Vitro* **2013,** *27*, (5), 1596-601.
38. Wang, K.; Ma, J. Y.; Li, M. Y.; Qin, Y. S.; Bao, X. C.; Wang, C. C.; Cui, D. L.; Xiang, P.; Ma, L. Q., Mechanisms of Cd and Cu induced toxicity in human gastric epithelial cells: Oxidative stress, cell cycle arrest and apoptosis. *Sci Total Environ* **2021,** *756*, 143951.
39. Wang, X.; Wang, W.-X., Cu(I)/Cu(II) released by Cu nanoparticles revealed differential cellular toxicity related to mitochondrial dysfunction. *Environ Sci Technol* **2023,** *57*, (26), 9548-9558.
40. Kuo, Y. M.; Gybina, A. A.; Pyatskowit, J. W.; Gitschier, J.; Prohaska, J. R., Copper transport protein (Ctr1) levels in mice are tissue specific and dependent on copper status. *J Nutr* **2006,** *136*, (1), 21-6.
41. Page, M. D.; Kropat, J.; Hamel, P. P.; Merchant, S. S., Two Chlamydomonas CTR copper transporters with a novel cys-met motif are localized to the plasma membrane and function in copper assimilation. *Plant Cell* **2009,** *21*, (3), 928-43.
42. Clifford, R. J.; Maryon, E. B.; Kaplan, J. H., Dynamic internalization and recycling of a metal ion transporter: Cu homeostasis and CTR1, the human Cu^{+} uptake system. *J Cell Sci* **2016,** *129*, (8), 1711-21.
43. Gunshin, H.; Mackenzie, B.; Berger, U. V.; Gunshin, Y.; Romero, M. F.; Boron, W. F.; Nussberger, S.; Gollan, J. L.; Hediger, M. A., Cloning and characterization of a mammalian proton-coupled metal-ion transporter. *Nature* **1997,** *388*, (6641), 482-8.
44. Arredondo, M.; Mendiburo, M. J.; Flores, S.; Singleton, S. T.; Garrick, M. D., Mouse divalent metal transporter 1 is a copper transporter in HEK293 cells. *Biometals* **2014,** *27*, (1), 115-23.
45. Komjarova, I.; Bury, N. R., Evidence of common cadmium and copper uptake routes in zebrafish *Danio rerio*. *Environ Sci Technol* **2014,** *48*, (21), 12946-51.
46. Pham, A. N.; Xing, G.; Miller, C. J.; Waite, T. D., Fenton-like copper redox chemistry revisited: Hydrogen peroxide and superoxide mediation of copper-catalyzed oxidant production. *J Catal* **2013,** *301*, 54-64.

664 47. Cheignon, C.; Collin, F.; Faller, P.; Hureau, C., Is ascorbate Dr Jekyll or Mr Hyde in the
665 Cu(Abeta) mediated oxidative stress linked to Alzheimer's disease? *Dalton Trans* **2016,** *45*,
666 (32), 12627-31.
667 48. Santoro, A.; Calvo, J. S.; Peris-Diaz, M. D.; Krezel, A.; Meloni, G.; Faller, P., The
668 glutathione/metallothionein system challenges the design of efficient O_2 -activating copper
669 complexes. *Angew Chem Int Ed Engl* **2020,** *59*, (20), 7830-7835.
670 49. Beswick, P. H.; Hall, G. H.; Hook, A. J.; Little, K.; McBrien, D. C.; Lott, K. A., Copper
671 toxicity: evidence for the conversion of cupric to cuprous copper in vivo under anaerobic
672 conditions. *Chem Biol Interact* **1976,** *14*, (3-4), 347-56.
673 50. Subramanian, A.; Tamayo, P.; Mootha, V. K.; Mukherjee, S.; Ebert, B. L.; Gillette, M. A.;
674 Paulovich, A.; Pomeroy, S. L.; Golub, T. R.; Lander, E. S.; Mesirov, J. P., Gene set enrichment
675 analysis: a knowledge-based approach for interpreting genome-wide expression profiles. *Proc*
676 *Natl Acad Sci U S A* **2005,** *102*, (43), 15545-50.
677 51. Ohgami, R. S.; Campagna, D. R.; McDonald, A.; Fleming, M. D., The Steap proteins are
678 metalloreductases. *Blood* **2006,** *108*, (4), 1388-94.
679 52. Knutson, M. D., Steap proteins: implications for iron and copper metabolism. *Nutr Rev*
680 **2007,** *65*, (7), 335-40.
681 53. Georgatsou, E.; Mavrogiannis, L. A.; Fragiadakis, G. S.; Alexandraki, D., The yeast
682 Fre1p/Fre2p cupric reductases facilitate copper uptake and are regulated by the copper-
683 modulated Mac1p activator. *J Biol Chem* **1997,** *272*, (21), 13786-92.
684 54. Attar, N.; Campos, O. A.; Vogelauer, M.; Cheng, C.; Xue, Y.; Schmollinger, S.; Salwinski,
685 L.; Mallipeddi, N. V.; Boone, B. A.; Yen, L.; Yang, S.; Zikovich, S.; Dardine, J.; Carey, M. F.;
686 Merchant, S. S.; Kurdistani, S. K., The histone H3-H4 tetramer is a copper reductase enzyme.
687 *Science* **2020,** *369*, (6499), 59-64.
688 55. Marckmann, D.; Trasnea, P. I.; Schimpf, J.; Winterstein, C.; Andrei, A.; Schmollinger, S.;
689 Blaby-Haas, C. E.; Friedrich, T.; Daldal, F.; Koch, H. G., The cbb_3-type cytochrome oxidase
690 assembly factor CcoG is a widely distributed cupric reductase. *Proc Natl Acad Sci U S A* **2019,**
691 *116*, (42), 21166-21175.
692 56. Kropat, J.; Gallaher, S. D.; Urzica, E. I.; Nakamoto, S. S.; Strenkert, D.; Tottey, S.; Mason,
693 A. Z.; Merchant, S. S., Copper economy in Chlamydomonas: prioritized allocation and
694 reallocation of copper to respiration vs. photosynthesis. *Proc Natl Acad Sci U S A* **2015,** *112*,
695 (9), 2644-51.
696 57. La Fontaine, S.; Quinn, J. M.; Nakamoto, S. S.; Page, M. D.; Gohre, V.; Moseley, J. L.;
697 Kropat, J.; Merchant, S., Copper-dependent iron assimilation pathway in the model
698 photosynthetic eukaryote *Chlamydomonas reinhardtii*. *Eukaryot Cell* **2002,** *1*, (5), 736-57.
699 58. Sakurai, T.; Kataoka, K., Basic and applied features of multicopper oxidases, CueO,
700 bilirubin oxidase, and laccase. *Chem Rec* **2007,** *7*, (4), 220-9.
701 59. Singh, S. K.; Roberts, S. A.; McDevitt, S. F.; Weichsel, A.; Wildner, G. F.; Grass, G. B.;
702 Rensing, C.; Montfort, W. R., Crystal structures of multicopper oxidase CueO bound to
703 copper(I) and silver(I): functional role of a methionine-rich sequence. *J Biol Chem* **2011,** *286*,
704 (43), 37849-57.
705 60. Shi, X.; Stoj, C.; Romeo, A.; Kosman, D. J.; Zhu, Z., Fre1p Cu^{2+} reduction and Fet3p Cu^{1+}

706 oxidation modulate copper toxicity in *Saccharomyces cerevisiae*. *J Biol Chem* **2003,** *278*, (50),
707 50309-15.
708 61. Stoj, C.; Kosman, D. J., Cuprous oxidase activity of yeast Fet3p and human ceruloplasmin:
709 implication for function. *FEBS Lett* **2003,** *554*, (3), 422-6.
710 62. Pilon, M.; Abdel-Ghany, S. E.; Cohu, C. M.; Gogolin, K. A.; Ye, H., Copper cofactor
711 delivery in plant cells. *Curr Opin Plant Biol* **2006,** *9*, (3), 256-63.
712 63. Contreras, L.; Moenne, A.; Gaillard, F.; Potin, P.; Correa, J. A., Proteomic analysis and
713 identification of copper stress-regulated proteins in the marine alga *Scytosiphon gracilis*
714 (Phaeophyceae). *Aquat Toxicol* **2010,** *96*, (2), 85-9.
715 64. Ritter, A.; Dittami, S. M.; Goulitquer, S.; Correa, J. A.; Boyen, C.; Potin, P.; Tonon, T.,
716 Transcriptomic and metabolomic analysis of copper stress acclimation in *Ectocarpus*
717 *siliculosus* highlights signaling and tolerance mechanisms in brown algae. *BMC Plant Biol*
718 **2014,** *14*, 116.
719 65. Chen, M.; Fang, X.; Wang, Z.; Shangguan, L.; Liu, T.; Chen, C.; Liu, Z.; Ge, M.; Zhang,
720 C.; Zheng, T.; Fang, J., Multi-omics analyses on the response mechanisms of 'Shine Muscat'
721 grapevine to low degree of excess copper stress (Low-ECS). *Environ Pollut* **2021,** *286*, 117278.
722 66. Hanikenne, M.; Motte, P.; Wu, M. C. S.; Wang, T.; Loppes, R.; Matagne, R. F., A
723 mitochondrial half-size ABC transporter is involved in cadmium tolerance in *Chlamydomonas*
724 *reinhardtii*. *Plant, Cell & Environment* **2005,** *28*, (7), 863-873.
725 67. Jamar, N. H.; Kritsiligkou, P.; Grant, C. M., Loss of mRNA surveillance pathways results
726 in widespread protein aggregation. *Sci Rep* **2018,** *8*, (1), 3894.
727
728